HHS Public Access

Author manuscript

Mol Imaging Biol. Author manuscript; available in PMC 2021 October 01.

Published in final edited form as:

Mol Imaging Biol. 2020 October ; 22(5): 1266–1279. doi:10.1007/s11307-020-01504-w.

Evaluation of Diagnostic Accuracy Following the Coadministration of Delta-Aminolevulinic-Acid and Second-Window Indocyanine-Green in Rodent and Human Glioblastomas

Steve S. Cho[1,2], **Saad Sheikh**[3], **Clare W. Teng**[1,2], **Joseph Georges**[4,5], **Andrew I. Yang**[1], **Emma De Ravin**[1,2], **Love Buch**[1], **Carrie Li**[1,2], **Yash Singh**[1], **Denah Appelt**[4], **Edward J. Delikatny**[6], **E. James Petersson**[7], **Andrew Tsourkas**[8], **Jay Dorsey**[3], **Sunil Singhal**[9], **John Y.K. Lee**[1]

[1]Department of Neurosurgery, Hospital of the University of Pennsylvania, Philadelphia, PA

[2]Perelman School of Medicine at the University of Pennsylvania, Philadelphia, PA

[3]Department of Radiation Oncology, Hospital of the University of Pennsylvania, Philadelphia, PA

[4]Department of Biomedical Sciences, Philadelphia College of Osteopathic Medicine, Philadelphia, PA

[5]Department of Neurosurgery, Philadelphia College of Osteopathic Medicine, Philadelphia, PA

[6]Department of Radiology, University of Pennsylvania, Philadelphia, PA

[7]Department of Chemistry, University of Pennsylvania, Philadelphia, PA

[8]Department of Bioengineering, University of Pennsylvania, Philadelphia, PA

[9]Department of Surgery, Hospital of the University of Pennsylvania, Philadelphia, PA

Abstract

Purpose: Fluorescence-guided-surgery offers intraoperative visualization of neoplastic tissue. Delta-aminolevulinic-acid (5-ALA), which targets enzymatic abnormality in neoplastic cells, is the only approved agent for fluorescence-guided neurosurgery. More recently, we described Second-Window-Indocyanine-Green (SWIG) which targets neoplastic tissue through enhanced vascular permeability. We hypothesized that SWIG would demonstrate similar clinical utility in identification of high-grade gliomas compared to 5-ALA.

Procedures: Female C57/BL6 and nude/athymic mice underwent intracranial implantation of 300,000 GL261 and U87 cells, respectively. Tumor-bearing mice were euthanized after administration of 5-ALA (200mg/kg intraperitoneal) and SWIG (5mg/kg intravenous). Brain

Corresponding author: John Y.K. Lee, MD, MSCE., Address: 801 Spruce Street, Philadelphia, PA 19107, Phone: 215-829-6700, Fax: 215-829-6645, leejohn@uphs.upenn.edu.

Authorship Statement: All authors have read and approved this manuscript.

Disclosures: JYKL has had stock options in VisionSense in the past. No other author disclosures or conflicts of interest.

Clinical Trial: NCT02710240 (US National Library of Medicine Registry; https://www.clinicaltrials.gov/ct2/show/NCT02710240?id=NCT02710240&draw=2&rank=1)

sections were imaged for protoporphyrin-IX and ICG fluorescence. Fluorescence and H&E images were registered using semi-automatic scripts for analysis. Human subjects with HGG were administered SWIG (2.5mg/kg intravenous) and 5-ALA (20mg/kg oral). Intraoperatively, tumors were imaged for ICG and protoporphyrin-IX fluorescence.

Results: In non-necrotic tumors, 5-ALA and SWIG demonstrated 90.2% and 89.2% tumor accuracy (p-value=0.52) in U87-tumors and 88.1% and 87.7% accuracy (p-value=0.83) in GL261-tumors. The most distinct difference between 5-ALA and SWIG distribution was seen in areas of tumor-associated necrosis, which often showed weak/no protoporphyrin-IX fluorescence, but strong SWIG fluorescence. In twenty biopsy specimens from four subjects with HGG, SWIG demonstrated 100% accuracy, while 5-ALA demonstrated 75–85% accuracy; there was 90% concordance between SWIG and 5-ALA fluorescence.

Conclusion: Our results provide the first direct comparison of the diagnostic utility of SWIG versus 5-ALA in both rodent and human HGG. Given the broader clinical utility of SWIG compared to 5-ALA, our data supports the use of SWIG in tumor surgery to improve the extent of safe resections.

Keywords

Fluorescence-guided surgery; 5-ALA; Second-Window ICG; Near-Infrared; High grade glioma

INTRODUCTION

Cancer remains a leading cause of death in the United States. While the medical community continues to develop novel medical treatments, surgical resection still plays a major role in the diagnosis, treatment, and palliation of most solid cancers. In tumors of the central nervous system, for instance, numerous studies have demonstrated that increasing the extent of resection is independently associated with improved patient outcomes.[1,2] Thus, resecting neoplastic tissue while preserving surrounding normal tissue is a critical task.

Surgeons rely on white-light illumination to assist with intraoperative visual differentiation of tumors from surrounding tissue. Additional tools, such as neuronavigation, intraoperative magnetic resonance imaging (MRI), intraoperative pathology, and/or intraoperative ultrasound are also used.[3,4] However, each of these modalities have significant drawbacks, such as: brain-shift that can significantly affect neuronavigation accuracy; low availability, high cost, and high false-positive rate with intraoperative MRI; and difficult and lengthy interpretation of ultrasound that disturbs operative workflow.[3–7] Recently, fluorescence-guided surgery (FGS) has emerged as a rapid and cost-effective alternative. In FGS, tumor-targeting fluorophores accumulate in neoplastic tissue and can be visualized in real-time intraoperatively.

Currently, delta-aminolevulinic-acid (5-ALA) is the only FDA-approved agent for FGS and is approved for high-grade gliomas (HGG) and bladder cancer.[8–11] 5-ALA is an oral prodrug that leads to selective accumulation of protoporphyrin-IX (PpIX; peak excitation 400–410nm, peak emission 635nm) in high-grade neoplastic cells.[9] 5-ALA has demonstrated >95% positive-predictive value for detecting neoplastic cells and has been associated with

increased resection rates and improved progression-free survival in patients with HGG.[8,9] On the other hand, the negative-predictive value (NPV) with 5-ALA for ruling out the presence of neoplastic tissue is very low, with most studies demonstrating NPV<25%.

Visible wavelength spectrum fluorophores, such as PpIX, have limitations that may reduce sensitivity. First, photons of visible wavelengths (400–700nm) are highly absorbed by endogenous fluorophores, such as hemoglobin, and have poor tissue penetration.[12,13] Thus, if neoplastic tissue is obscured under just 1mm of tissue, no fluorescence is elicited, and the neoplastic tissue may be missed. Second, numerous endogenous fluorophores in the body (i.e. flavin, collagen, heme, lipofuscin, etc.) fluoresce in the visible spectrum, leading to background signal, ultimately reducing the contrast between the fluorescent neoplastic tissue and the background normal tissue.[14,15] In addition, PpIX has poor quantum efficiency and low extinction coefficient and is a relatively dark fluorophore.[16]

Given these limitations of visible-spectrum fluorophores, the near-infrared (NIR) spectrum (700–900nm) is appealing. NIR fluorescence benefits from enhanced tissue penetration by photons due to limited absorption by endogenous fluorophores and also from decreased background auto-fluorescence, giving NIR fluorescence greater contrast.[12] To take advantage of NIR fluorescence, multiple groups are investigating novel NIR fluorophores conjugated to antibodies, affibodies, or small molecules targeting various receptors on cancer cells.[17–22]

We have pioneered a novel application of the FDA-approved NIR fluorophore, indocyanine-green (ICG; peak excitation 805nm, peak emission 835nm). Conventionally, ICG is used as an intraoperative angiographic agent (0.350mg/kg). In our Second-Window-ICG (SWIG) technique, ICG is instead administered intravenously at a high dose (2.5–5mg/kg). Over a 24-hour time window, ICG accumulates in areas of epithelial damage and enhanced vascular permeability, such as in peritumoral areas, via the enhanced-permeability-and-retention (EPR) effect. In addition, there is evidence that ICG accumulates intracellularly in neoplastic cells via endocytosis after EPR accumulation, resulting in prolonged, tumor-specific retention.[23] Our group has previously demonstrated high sensitivity (>90%) and NPV (>70%) for detecting neoplastic tissue in intracranial tumors (gliomas, meningiomas, metastases, and pituitary adenomas) using SWIG.[24–29] The two main advantages of SWIG over other NIR contrast agents are that ICG is FDA-approved, facilitating clinical utility, and that it is widely applicable to multiple tumor types, unlike receptor-targeting dyes.

In this study, we compare 5-ALA and SWIG in two independent murine models of intracranial HGG, as well as human subjects with HGG. Prior studies suggest that 5-ALA has higher specificity for neoplastic tissue while SWIG has higher sensitivity; however, there have been no direct comparisons of these two techniques, which are currently the only agents available for fluorescence-guided neurosurgery.

METHODS

PRECLINICAL EXPERIMENTS

Cell Lines and Culture Methods—GL261-Luciferase and U87-luciferase cells (gift from Dorsey Lab) were cultured in DMEM (ThermoFisher, Carlsbad, CA) or Modified IMEM (ThermoFisher, Carlsbad, CA), respectively (+10% fetal bovine serum, 100 units/mL Penicillin, and 100 μg/mL Streptomycin) in a humidified incubator at 37°C and 5% CO_2. Cells were certified mycoplasma-free by the MycoAlert® Assay (Cambrex, East Rutherford, NJ) on a regular basis (last test November 2019). Cells were passaged 2–3 times prior to stereotactic implantation.

Orthotopic Mouse Glioma Model—All animal procedures were conducted according to a protocol approved by the Institutional Animal Care and Use Committee at the University of Pennsylvania (#805979) and NIH and ARRIVE guidelines. Female mice (*Mus musculus* C57/BL6 strain and nude, athymic) at 6 weeks of age (Charles River Laboratories, Wilmington, MA) underwent orthotopic implantation of intracranial tumors, sham procedures, or no procedures.

Orthotopic implantation followed a protocol as previously described.[30] Briefly, mice were shaved at the head, anesthetized using 1–4% isoflurane, immobilized in a stereotactic device (Stoelting, Wood Dale, IL), and incised along the scalp midline. A burr hole was placed on the right side 3mm lateral to the midline and 3mm posterior to the bregma. A 10uL syringe (Hamilton Co., Reno, NV) was inserted through this hole to a depth of 3.5mm from the brain surface. Three microliters of 100,000cells/uL were injected through the syringe at a rate of 0.5uL/minute. After needle withdrawal, the skull was cleaned with 70% ethanol and the scalp was closed with skin glue. Sham animals underwent the identical surgical procedure with sterile PBS; animals were not randomized to sham or tumor implantation.

One week after implant, mice underwent in-vivo bioluminescence imaging after intraperitoneal injections of 150mg/kg luciferin (Gold Biotechnology, St Louis, MO) to confirm successful tumor implantation. Mice were then monitored during tumor growth until they showed early signs of illness (weight loss >20%, lethargy, or abnormal motor activity).

Fluorescence Imaging—At the first sign of illness, ICG (Akorn, Lake Forest, IL) was administered intravenously at 5mg/kg via the tail veins. Approximately 20-hours later, 5-ALA (Sigma Aldrich, St. Louis, MO) was delivered intraperitoneally at 200mg/kg. Then, 3–3.5 hours later, the mice were humanely euthanized. Their brains were harvested and sectioned coronally through the middle of the tumor. Slices were placed on microscope slides and imaged on the Odyssey CLx-1 (Li-Cor Biosciences, Lincoln, NE) flatbed laser scanner to capture the distribution of ICG at 21um pixel resolution using the 800-emission channel (785nm excitation laser), which does not introduce cross-excitation of PpIX. Then, slices were placed under a dissecting microscope attached to a high-resolution camera (Canon EOS Rebel T2i) and were imaged either under white-light with no filter or under blue-light excitation (395–405nm light-emitting diode) with a 610–690nm emission filter (Thorlabs, Newton, NJ).

Histopathology—Following fluorescence imaging, the brain sections were fixed in formalin, embedded in paraffin blocks, and sliced in 5um thickness prior to fixing onto glass slides. All slides underwent hematoxylin-eosin (H&E) staining.

Image Registration and Region-of-Interest Analysis—Registration of the fluorescence images and H&E slides was completed using custom scripts (Matlab, MathWorks, MA, USA) adapted from previously-published methodology.[19] The steps are briefly outlined here, with pertinent Matlab functions provided in parentheses. First, all three images (ICG, PpIX, H&E) were resized based on pixel resolutions. Binary masks of the tissue slices were then created on all three images using pre-defined thresholds and refined manually as needed. Binary masks of the two fluorescence images were then registered using a rigid transformation (*imregconfig, imregtform, imwarp*). As the first of a two-step process, the H&E mask was registered to the fluorescence masks using an affine transformation. The tumor was then manually segmented on the H&E section, and its center-of-mass was identified (*regionprops*). Thirty radial lines spaced 12 degrees apart were projected from the tumor center to the tissue boundary, and the intersecting points were used as control points for the second-step registration using a non-rigid B-spline registration (*bspline_transform*, open source package from MathWorks File Exchange). This two-step registration attempts to account for non-rigid tissue deformation that occurs during formalin fixation.

The co-registered images were then imported into ImageJ (NIH, Bethesda, MD) and overlaid using the *Merge Channels* function. Twenty regions of interest (ROI), each one approximately 0.5% of the cross-sectional area, were then randomly selected from within 5mm of the tumor core using a random number generator for the coordinates. The fluorescence intensity at each channel within each ROI was measured using ImageJ. By using the H&E section to find an area of normal white-matter, background signal intensity was measured and was used to calculate the signal-to-background-ratio (SBR) for ICG and PpIX fluorescence within each ROI. Furthermore, the underlying H&E within each ROI was examined to determine whether neoplastic cells were present, and each ROI was labeled yes/no for tumor presence; for tumors with significant necrosis, necrotic areas were considered neoplastic if there were dysplastic cells.

Fluorescence Accuracy Assessment—Using the above ROI data, a receiver-operating-characteristic (ROC) curve was constructed for ICG and 5-ALA. Area under the ROC curves were used to calculate the accuracy for each fluorophore and the optimal SBR to maximize the accuracy was calculated.

CLINICAL TRIAL

Study Population—Adult patients (>18 years) undergoing resection of primary or recurrent HGG were enrolled beginning in January 2019 in a registered trial that was approved by the University of Pennsylvania's Institutional Review Board (NCT02710240). Exclusion criteria were pregnancy, porphyria, and/or allergy to contrast dye, iodide or shellfish. All patients gave informed consent.

Fluorophore Administration—Approximately 24 hours prior to scheduled surgery, patients were infused intravenously with 2.5mg/kg of ICG (C43H47N2O6S2.Na; Akorn Pharmaceuticals, Illinois, USA). Then 3 hours prior to surgery, patients were given 20mg/kg of 5-ALA (Gleolan NX Development Corp, Kentucky, USA) in water or juice to drink.

Fluorescence Imaging—For NIR fluorescence, all cases were imaged using the FDA-approved VisionSense Iridium™ exoscope (VisionSense, Philadelphia, PA) with a 805nm laser excitation source and picomolar sensitivity for NIR contrast agents.[31,32]

For PpIX fluorescence, a Leica OH6 microscope with the FL400 module (Leica, Wetzlar, Germany) was used, which uses a bandpass filter (380–430nm) over the existing Xenon white-light to provide blue-light excitation and a >444nm long-pass filter for emission.

Surgical Procedure—Standard-of-care resections were performed as previously described.[24] Upon craniectomy, NIR and PpIX fluorescence were imaged over the intact dura. The dura was then opened and fluorescence was measured. For deep tumors, fluorescence was measured again following corticectomy to reveal the tumor. When the attending neurosurgeon achieved satisfactory resection using white-light and microscope visualization alone, fluorescence imaging was used to identify areas of residual fluorescence. Margin biopsies were performed at the discretion of the senior surgeon, and the specimens were sent to pathology.

Fluorescence Image Analysis—Time-lapse recordings of the tumor resections were analyzed postoperatively by independent reviewers (SSC, LB). The presence or absence of NIR signal, as well as the SBR was analyzed at all views as in prior studies.[32] NIR SBR greater than 2.0 was deemed significant, based on our prior intraoperative experiences. For 5-ALA signal, all specimens were subjectively graded (none/weak/strong) for red fluorescence intensity by the senior surgeon at the time of biopsy, consistent with most 5-ALA literature.

Statistical Analysis—All statistical analyses were performed using STATA 10™ (StataCorp LLC, CollegeStation, TX). Comparisons between fluorescence imaging were performed using the nonparametric sign-test for matched pairs. Area under the ROC curves for each condition was calculated using the *roccomp* function in STATA. P-value<0.05 was predetermined to be the cutoff for designating statistical significance.

RESULTS

Preclinical Murine Model of HGG

A total of 34 mice were used in this study (17 GL261 tumors, 11 U87 tumors, 3 sham injections, and 3 control mice). Brains from 3 of the 28 tumor-bearing mice were harvested without administration of either 5-ALA or ICG to investigate auto-fluorescence. The remaining 31 mice all received both 5-ALA and ICG.

All 28 mice successfully developed invasive tumors. Of the 25 mice with intracranial tumors that received 5-ALA and ICG, 47 coronal slices were successfully recovered, with 3 lost

during tissue processing. On H&E, the U87 tumors accounted for 25.3±5.2% of the coronal area; there were no significantly necrotic tumors. The GL261 tumors, in contrast, had 5 necrotic tumors of the 14. The 9 non-necrotic tumors (31.1±6.5%) were significantly smaller than the necrotic tumors (43.3±3.5%, p-value=0.001). On H&E, the tumor core in these necrotic tumors demonstrated tissue necrosis but also demonstrated the presence of neoplastic cells with dysmorphic features. The sham-procedure and control mice did not develop any tumors.

Fluorescence Imaging in the Murine Model

All 47 coronal slices from tumor-bearing mice, both U87 and GL261, that received 5-ALA and ICG demonstrated tumor fluorescence under both blue-light and NIR excitation (Figure 1). However, all 10 coronal slices from mice with grossly necrotic GL261 tumors demonstrated an area of minimal PpIX fluorescence in the tumor core (SBR=1); in contrast, strong ICG signal (SBR>2.0) was found throughout these tumors (Figure 1E–H). In some mice, ICG signal with SBR>2.0 was also found in the lateral ventricles and/or the needle tract from the tumor implantation procedure (Figure 1D).

In order to explore non-tumor uptake of ICG and 5-ALA, 6 coronal brain slices from 3 control mice with no intracranial tumors were imaged after 5-ALA and SWIG administration (Figure 2A–D). Strong PpIX fluorescence (SBR>2.0) was observed in the hippocampal formation, while moderate PpIX fluorescence (SBR 1.5–2.0) was observed in the corpus callosum, although the absolute signal intensity was 4-fold lower than in the tumor-bearing mice. Strong ICG fluorescence (SBR>2.0) was observed in the lateral ventricles at similar absolute intensity to the tumor-bearing mice, while moderate fluorescence (SBR 1.5–2.0) was noted in the third ventricle and the horns of the lateral ventricles. H&E staining revealed choroid plexus in these areas.

Finally, 6 coronal slices from the 3 tumor-bearing mice that did not receive 5-ALA or ICG demonstrated diffuse autofluorescence throughout the brain under blue-light excitation and no significant autofluorescence under NIR excitation (Figure 2E–H).

Fluorophore Accuracy for Detecting Neoplasm in Orthotopic U87

In the 20 coronal slices from 11 U87-tumor-bearing mice, a total of 400 ROIs were randomly sampled from within 5mm of the tumor core (209 neoplastic, 191 non-neoplastic on H&E). The fluorescence SBR was significantly higher for neoplastic specimens (5-ALA median SBR=2.32vs1.18; SWIG median SBR=4.21vs1.62). Area under the ROC curve was 0.902 for 5-ALA (95% CI 0.870–0.935) and 0.892 for SWIG (95% CI 0.857–0.926) (Figure 3A, p-value=0.52).

With the above ROC analysis, the optimal SBR cutoff for 5-ALA and SWIG were calculated. For 5-ALA, an SBR cutoff of 1.7 led to 92.8% sensitivity and 82.2% specificity, with an overall 87.8% correct characterization. For SWIG, an SBR cutoff of 2.2 led to 95.7% sensitivity, 75.9% specificity, with an overall 86.8% correct characterization. Using these SBR cutoffs, 351/400 of the ROIs (87.5%) demonstrated concordance between 5-ALA and SWIG (211 positive for both, 140 negative for both; chi-2 p-value<0.0001). Of the 49

discordant ROIs, 32 demonstrated SWIG fluorescence-only and 17 demonstrated 5-ALA fluorescence-only.

In order to achieve >95% tumor specificity, an SBR cutoff of 2.7 for 5-ALA (35.9% sensitivity) and 4.6 for SWIG (33.0% sensitivity) were necessary.

Fluorophore Accuracy for Detecting Neoplasm in Orthotopic GL261

In the 27 coronal slices from 14 GL261-tumor-bearing mice, a total of 540 ROIs were randomly sampled from within 5mm of the tumor core (297 neoplastic, 243 non-neoplastic on H&E). ROIs containing some necrosis or other non-neoplastic cells were considered neoplastic if they included dysplastic tumor cells on microscopy. The fluorescence SBR was significantly higher for neoplastic specimens (5-ALA median SBR=2.17vs1.27; SWIG median SBR=4.41vs1.65).

On gross tumor fluorescence visualization, necrotic tumors demonstrated significantly lower signal in the core. Thus, a stratified analysis was performed by tumor necrotic status. In 17 brain slices that were minimally/non-necrotic under white-light visualization, area under the ROC curve was 0.881 for 5-ALA (95% CI 0.844–0.919) and 0.877 for SWIG (95% CI 0.841–0.914) (Figure 3B, p-value=0.83). In contrast, in 10 brain slices that were grossly necrotic under white-light, 5-ALA had a significantly lower area under the ROC curve (0.712; 95% CI 0.640–0.783) compared to SWIG (0.861; 95% CI 0.796–0.927) (Figure 3C, p-value<0.0001). The accuracy of 5-ALA in necrotic tumors was significantly lower than the accuracy of 5-ALA in non-necrotic tumors (0.712 vs 0.881; p-value<0.0001); for SWIG, there was no difference in accuracy between necrotic and non-necrotic tumors (p-value=0.67).

Using the ROC analysis in non-necrotic tumors, the optimal SBR cutoff for 5-ALA and SWIG in GL261 tumors were calculated. For 5-ALA, an SBR cutoff of 1.9 led to 86.5% sensitivity and 80.4% specificity, with an overall 83.5% correct characterization. For SWIG, an SBR cutoff of 2.5 led to 88.5% sensitivity, 75.0% specificity, with an overall 81.2% correct characterization. Using these SBR cutoffs in the 17 non-necrotic tumors, 291/340 of the ROIs (85.6%) demonstrated concordance between 5-ALA and SWIG (151 positive for both, 140 negative for both; chi-2 p-value <0.0001). Of the 49 discordant ROIs, 30 demonstrated SWIG fluorescence-only and 19 demonstrated 5-ALA fluorescence-only. In the 10 necrotic tumors, only 113/200 of the ROIs (56.5%) demonstrated concordance (56 positive for both, 57 negative for both; p-value<0.0001). Of the 87 discordant ROIs, 80 demonstrated SWIG fluorescence-only and 7 demonstrated 5-ALA fluorescence-only.

In order to achieve >95% tumor specificity in non-necrotic tumors, SBR cutoffs of 2.7 for 5-ALA (33.3% sensitivity) and 5.0 for SWIG (29.5% sensitivity) were necessary.

NIR Fluorescence in Necrotic Tissue – Clinical Study

To explore the distribution of ICG into necrotic tissue that we observed in the murine model, we retrospectively examined imaging data from four patients with a history of HGG who underwent repeat resections of contrast-enhancing lesions concerning for recurrence under the SWIG protocol. In all four patients, pathologic analysis of their specimens demonstrated

no viable tumor cells and instead yielded “radiation necrosis and treatment-related changes, with no recurrent neoplasm”. Overall, 9 specimens containing abnormal tissue (radiation necrosis, inflammation, or other changes) were biopsied, and NIR fluorescence was positive for 8 specimens (SBR=8.2±4.5). The NIR fluorescence intensity and quality was indistinguishable from those obtained from other patients with actual HGG.

Human Intraoperative Dual-Fluorophore Visualization

Four patients with HGG (3 primary, 1 recurrent) underwent resection after receiving both SWIG and 5-ALA (Figure 4). Intraoperatively, fluorescence imaging was performed before and after durotomy and for each biopsy specimen. As expected based on prior publications,[24,27] NIR imaging with SWIG localized the tumors prior to durotomy, but blue-light excitation did not demonstrate any red fluorescence prior to durotomy (Figure 4A–C). Upon tumor exposure (Figure 4D–F), all tumors demonstrated strong (none/weak/strong) 5-ALA fluorescence and high ICG SBR (6.1±1.5). All 4 tumors demonstrated HGG on pathology (Figure 4G).

In total, 20 specimens were biopsied (Table 1). Of the 20 specimens, 13 specimens demonstrated both strong 5-ALA fluorescence and NIR SBR >2.0; these were all neoplastic on pathology. Two specimens demonstrated NIR SBR >2.0 but only weak 5-ALA fluorescence; these specimens were both neoplastic on pathology. Three specimens demonstrated no 5-ALA and no NIR fluorescence and were all non-neoplastic. Finally, two specimens demonstrated discordance between 5-ALA and ICG fluorescence (bold and italicized in Table 1). One specimen was negative for 5-ALA but positive for ICG (Figure 4H–J; white, notched arrow); the specimen was neoplastic on pathology (Figure 4K), although there was also a significant amount of necrosis. Another specimen was strongly positive for 5-ALA but negative for ICG (Figure 4H–J; white arrow); the specimen demonstrated reactive brain parenchyma without any neoplastic cells (Figure 4L).

Overall, white-light identification of tissue correctly classified tissue into neoplastic/non-neoplastic in 15/20 specimens (75%). 5-ALA fluorescence correctly classified tissue in 17/20 specimens (85%) when weak fluorescence was used as the cutoff; using strong fluorescence only, this decreased to 15/20 (75%) – 2 additional specimens were partially necrotic and demonstrated weak PpIX fluorescence only. ICG fluorescence correctly classified tissue in all 20/20 specimens (100%), including the specimens containing necrosis mixed with neoplastic tissue.

DISCUSSION

FGS for solid tumors has garnered recent interest as an inexpensive and rapid method to increase intraoperative diagnostic accuracy. Since increased extent of resection is associated with decreased recurrence rates, improved symptomatic relief, and/or prolonged survival, FGS has the potential to improve surgical outcomes in solid tumors. This is of particular interest in neurosurgery, where complete resection while preserving valuable neurologic function can be difficult.

To effectively assess the utility of contrast agents, the distribution of fluorophores into neoplastic areas must be stringently assessed. Specifically, in clinical practice, it is often not the gross tumor that the surgeon has difficulty detecting, but rather, areas of residual neoplasm in the margins. However, accurately determining the extent of tumor on fluorescence images can be difficult and is highly dependent on proper alignment with histology images. A previous study by Elliott et al[19] addressed this potential issue by using a semi-automated algorithm to co-register histology images and fluorescence images to assess the distribution of fluorophores in the tumor margins as well as the tumor cores. Similarly, we co-registered the histology and fluorescence images using semi-automatic, non-rigid transformations. We then randomly selected ROIs within 5mm of the tumor center in order to sample the normal tissue, tumor margins, as well as the tumor cores, thus reducing the potential sampling bias.

Overall, we compared the utility of 5-ALA and SWIG in this translational study of FGS in HGG using two orthotopically implanted glioma cell lines (Table 2). Using two cell lines served as a measure of internal validity and generalizability of our findings.

SWIG and 5-ALA Demonstrate Similar Mechanism of Distribution

It has been proposed that although 5-ALA requires metabolic conversion to achieve fluorescence, it primarily relies on the EPR effect to first reach neoplastic cells.[33] Our data is consistent with this hypothesis; in two independent orthotopic murine glioma models using two glioma cell lines and in human tumors, there was >85% concordance between SWIG and 5-ALA.

Importantly, an area of significant difference between 5-ALA and SWIG distribution was in tissue with significant necrosis. In 10 GL261 tumor sections with significant central necrosis, the tumor cores fluoresced under NIR excitation after SWIG administration but not under blue-light excitation with 5-ALA administration. 5-ALA, unlike ICG, is a prodrug and must be converted to the fluorophore PpIX by neoplastic cells. Thus, in areas of tumor that are significantly infiltrated by necrosis, there are not enough neoplastic cells to lead to strong PpIX fluorescence. This lack of 5-ALA fluorescence in necrotic areas was also seen in a prior study that showed fluorescence in necrotic areas using an EGFR-targeting dye, but not with 5-ALA.[19] This factor likely contributed to the one false-negative specimen (neoplasm with necrosis infiltration) observed with 5-ALA in a human subject with recurrent HGG (Figure 4H–L).

In contrast, ICG is a fluorophore that needs no metabolic conversion and targets areas of damaged endothelium and blood-brain-barrier breakdown via the EPR effect. Since both neoplastic and necrotic areas lead to damaged and permeable endothelium,[34–36] SWIG leads to strong NIR fluorescence in both necrosis and neoplasm. We further assessed this effect in patients with radiation necrosis and/or treatment-related changes, whose biopsy specimens demonstrated strong NIR fluorescence after SWIG administration despite having no neoplastic cells on pathology. Although necrotic areas may not necessarily be neoplastic, they must still be resected during tumor surgery and thus, NIR imaging with SWIG offers a valuable adjunct in detecting these abnormal tissues for resection. Thus, in recurrent HGG,

which are often associated with significant necrosis interspersed with tumor, our data suggests that SWIG would be more sensitive than 5-ALA.

Overall, our data suggests that 5-ALA, like SWIG, primarily targets areas of damaged and permeable endothelium and that the potential increase in tumor-specificity conferred by enzymatic conversion to PpIX may not necessarily be seen in clinical practice.

SWIG and 5-ALA Accumulate in Specific Non-Neoplastic Tissues

We investigated sources of non-neoplastic fluorescence with 5-ALA and SWIG in the brain (Figure 2). In our murine model, PpIX fluorescence was observed in white matter tracts, specifically the hippocampal formation and the corpus callosum. Interestingly, the one false-positive finding with 5-ALA in human subjects occurred in a similar region, in the white matter near the cingulum (Figure 4H–L), which demonstrated strong PpIX fluorescence but no tumor cells on histopathology, suggesting this may be a concurrent finding in murine and human brains. The reason for this is unclear, and a literature search did not document similar findings. Thus, 5-ALA should be used with caution in periventricular tumors in order to avoid resection of benign, eloquent white matter. With SWIG, NIR signal was seen in mice brains, both with and without tumors, in the choroid plexus (lateral and third ventricles). It is well known that the choroid plexus is an area of permeable blood-brain barrier, which results in contrast-enhancement on MRI with gadolinium. Thus, it is expected that SWIG, which relies on the EPR effect like gadolinium, would also lead to fluorescence within the choroid plexus. Indeed, we have previously published a case report demonstrating strong SWIG signal in the normal choroid plexus.[37] Since the choroid plexus is easily distinguishable intraoperatively, we believe this would be a non-issue in FGS with SWIG. Non-tumor SWIG signal was also seen in some mice brains around the needle tract, likely due to the physical damage from the needle disrupting the blood-brain-barrier; this is not clinically relevant in human patients.

SWIG Offers Clinical Advantages Beyond 5-ALA

Effective FGS requires more than just tumor-specific fluorescence. For successful and safe surgery, surgeons must be able to easily visualize the fluorophore that has accumulated in the tumor while also maintaining perspective of the non-fluorescent background within the surgical area. Furthermore, the ability to detect neoplastic tissue that may be hidden under blood or normal tissue is crucial to reduce the chances of leaving residual neoplasm. In both regards, SWIG proves superior to 5-ALA.

ICG, unlike PpIX, excites and emits in the NIR spectrum, which allows much greater tissue penetration due to the virtual lack of endogenous fluorophores that absorb photons in that range.[12,13] Phantom studies and prior intraoperative imaging by our group demonstrate that NIR fluorescence can be detected through >1cm of soft tissue, such as the brain or dura.[24,25,27,38] In contrast, blue-light excitation used for PpIX fluorescence is obscured by <1mm of soft tissue or blood in the surgical field.[39] Figure 4A–C demonstrate the clinical implications of this finding. With conventional white-light imaging or blue-light excitation for PpIX, tumors that do not grossly deform the brain or invade the dura are impossible to visualize through the dura. However, with NIR imaging and SWIG, tumors are easily

localized through the intact dura, which can guide neurosurgeons in making safe and efficient openings in the dura and cortex to approach the tumor. Furthermore, residual neoplasm that may be hidden behind normal tissue, obscuring it from white-light or blue-light imaging, would be clearly visible with NIR imaging. Extracranially, this property of NIR imaging would still be beneficial, such as in the lungs or gastrointestinal organs, where the ability to detect non-superficial tumors using NIR imaging could greatly enhance the surgeons' abilities to localize and resect tumor nodules.

NIR imaging with SWIG also better preserves surrounding tissue visibility compared to 5-ALA. As depicted in Figure 4, 5-ALA FGS using commercial equipment must be performed under blue-light excitation; while the full visible-light spectrum includes 400nm and would partially excite PpIX, the resulting red fluorescence would not stand out in the surgical field. However, performing surgery under blue-light excitation is a challenging task for surgeons who are accustomed to operating using white-light illumination. This results in surgeons switching repeatedly between white-light and blue-light illumination, which disturbs the surgical workflow. In contrast, because there is no overlap between the visible and NIR spectrum, illumination can be performed in both spectrums simultaneously, and as a result, surgeons can perform FGS while maintaining optimal visualization of the surrounding tissue. While this overlay has been demonstrated with 5-ALA using a custom-made device,[39] this reduces tumor sensitivity even further. Additionally, ICG is a significantly brighter dye than 5-ALA (brightness 11,000 vs 400$M^{-1}cm^{-1}$).[16] Indeed, the enhanced sensitivity of tumor detection using ICG was demonstrated in a study of superficial liver tumors; despite the fact that ICG is metabolized by the liver (hence, accumulating in normal liver as well and causing more background signal than would be expected in the brain), the accuracy of tumor detection with ICG was 94% versus 58% for 5-ALA.[40]

SWIG Compared to Novel Near-Infrared Fluorophores

Most surgical investigators currently favor NIR fluorophores over visible-spectrum fluorophores. For instance, Van Dam et al proposed folate receptor alpha as a viable target for receptor-targeted FGS in ovarian cancers and demonstrated feasibility initially by synthesizing EC17, a folate analog linked to a visible-spectrum fluorophore[41]; however, this was soon replaced by OTL38, a folate analog linked to a NIR fluorophore, which is undergoing phase III trial in ovarian cancers and phase II trial in lung cancers.[42–45] Likewise, other groups are attempting to develop novel conjugated NIR agents that target various extracellular receptors in a tumor-specific manner.[46–49] These novel dyes are showing varying levels of promise in preclinical and clinical trials and may one day be an integral part of the oncologic surgeons' armamentarium.

Unlike the novel dyes, SWIG targets the permeable peritumoral environment to deliver ICG to the tumor cells. SWIG offers two main advantages over targeted agents. First, as an FDA-approved agent, ICG is nearly universally available and the SWIG protocol (2.5–5mg/kg intravenous infusion followed by NIR imaging 24-hours later) is easy to replicate. Thus, FGS using SWIG could easily be employed globally to enhance surgeons' ability to detect neoplastic tissue intraoperatively. More importantly, unlike the novel receptor-targeting agents, SWIG is widely applicable to a variety of tumors. For instance, EGFR-targeting

agents have been proposed for FGS in HGG resections[19,20]; however, approximately 40% of HGG are found to not overexpress EGFR and even within the same tumor margins, there is high heterogeneity in terms of EGFR expression, which would affect reliable FGS with EGFR-targeting agents.[50] Perhaps more importantly, tumor receptor expression levels are unknown until patients undergo biopsy or resection of their tumors, making it impossible to preemptively choose the patients in whom receptor-targeting agents would be useful.

In contrast, because SWIG relies on the EPR effect, which is a common quality found in most tumors, SWIG has demonstrated utility not only in HGGs, but also meningiomas, metastases, and pituitary adenomas intracranially, as well as lung cancers extracranially.[24–29,51] Indeed, other surgeons at our institution have observed that SWIG leads to tumor-specific fluorescence in peripheral nerve schwannomas and spinal meningiomas, suggesting that SWIG truly has a wide array of applications, unlike the novel, targeted dyes under development. Finally, because SWIG and gadolinium both rely on the EPR effect to accumulate in tumor tissue, surgeons can use preoperative MRI with gadolinium to select those patients in whom SWIG will yield useful fluorescence imaging.

While there certainly is value in increased tumor-specificity, SWIG's EPR mechanism of action offers significant and clinically relevant advantages over novel agents that are under development for NIR FGS.

Limitations

There are some limitations to this study. For the preclinical portion of this study, the experiments were carried out in mice with orthotopic brain tumors, which do not completely recapitulate true human HGGs. However, we used two HGG cell lines (U87 and GL261) in two strains of mice (nude athymic and C57/BL6) to create two, independent murine models of intracranial HGG. In both models, we found very similar results in terms of fluorophore accuracy, fluorophore SBR, and test characteristics (sensitivity/specificity). Furthermore, we enrolled human subjects in our study to validate the findings that were seen in the preclinical model, thus addressing some of this limitation.

As for the clinical portion of the study, we have enrolled only 4 patients to date, with a total of 20 biopsy specimens. Thus, we were not able to more thoroughly compare 5-ALA and SWIG in humans as we did in mice. A larger study in the future by enrolling more patients and administering 5-ALA and SWIG may better elucidate clinical differences between 5-ALA and SWIG.

Finally, in our study, we relied on simple optical fluorescence to determine 5-ALA and SWIG distribution. While surgeons currently rely on optical fluorescence in the operating room to measure fluorescence, it has been shown in research settings that other methods of fluorescence measurements, such as spectroscopy, are significantly more sensitive.[52,53] Thus, it is possible that with spectroscopy, we could have detected PpIX signal in areas that were not visualized in our study (i.e. in necrotic parts or in non-enhancing tissue); however, spectroscopy is not the standard of care, and thus, we chose to use optical fluorescence. Furthermore, we were not able to visualize fluorescence at the cellular resolution, as has been done by Onda et al.[23] The authors used sophisticated Olympus microscopes that are

beyond our group's capabilities in order to demonstrate colocalization of ICG and PpIX within cytoplasmic organelles in the HT-29 colon cancer cell line. Future analysis with this level of detail may further elucidate differences in tumor specificity between SWIG and 5-ALA.

CONCLUSION

Second-Window ICG, a novel application using the near-infrared fluorophore ICG, leads to tumor-specific accumulation of ICG via the EPR effect. In contrast, 5-ALA leads to selective accumulation of PpIX, a visible-spectrum fluorophore, in high-grade neoplastic cells. In rodents and humans with HGG, SWIG and 5-ALA both demonstrate highly accurate detection of neoplastic tissue. However, fluorescence imaging in the NIR spectrum has several advantages over visible-spectrum fluorescence imaging that enhances the clinical utility of SWIG over 5-ALA, suggesting that SWIG would be a valuable addition to the oncologic surgeons' armamentarium.

Acknowledgements

Financial Support: Supported in part by the National Institutes of Health R01 CA193556 (SS), and the Institute for Translational Medicine and Therapeutics of the Perelman School of Medicine at the University of Pennsylvania (JYKL). Research reported in this publication was also supported by the National Center for Advancing Translational Sciences of the National Institutes of Health under Award Number UL1TR000003 (JYKL). In addition, research reported in this publication was supported by the National Center for Advancing Translational Sciences of the National Institutes of Health under award number TL1TR001880 (SSC). The content is solely the responsibility of the authors and does not necessarily represent the official views of the NIH.

Abbreviations

5-ALA	delta-aminolevulinic-acid
FGS	fluorescence-guided surgery
H&E	Hematoxylin and eosin
HGG	high-grade glioma
ICG	indocyanine green
MRI	magnetic resonance imaging
NIR	near-infrared
NPV	negative predictive value
PpIX	protoporphyin-IX
ROC	receiver operating characteristic
ROI	region of interest
SBR	signal to background ratio
SWIG	Second-Window Indocyanine Green

REFERENCES

1. Lacroix M et al. A multivariate analysis of 416 patients with glioblastoma multiforme: prognosis, extent of resection, and survival. J. Neurosurg 95, 190–198 (2001).
2. Sanai N, Polley M-Y, McDermott MW, Parsa AT & Berger MS An extent of resection threshold for newly diagnosed glioblastomas. J. Neurosurg 115, 3–8 (2011). [PubMed: 21417701]
3. Wirtz CR et al. The benefit of neuronavigation for neurosurgery analyzed by its impact on glioblastoma surgery. Neurol. Res 22, 354–60 (2000). [PubMed: 10874684]
4. Sherman JH et al. Neurosurgery for Brain Tumors: Update on Recent Technical Advances. Curr. Neurol. Neurosci. Rep 11, 313–319 (2011). [PubMed: 21327735]
5. Berkmann S, Schlaffer S, Nimsky C, Fahlbusch R & Buchfelder M Intraoperative high-field MRI for transsphenoidal reoperations of nonfunctioning pituitary adenoma. J. Neurosurg 121, 1–10 (2014).
6. Kuo JS et al. Congress of Neurological Surgeons Systematic Review and Evidence-Based Guideline on Surgical Techniques and Technologies for the Management of Patients With Nonfunctioning Pituitary Adenomas. Neurosurgery 79, E536–E538 (2016). [PubMed: 27635962]
7. Sheehan J et al. Congress of Neurological Surgeons Systematic Review and Evidence-Based Guideline for the Management of Patients With Residual or Recurrent Nonfunctioning Pituitary Adenomas. Neurosugery 79, 539–540 (2016).
8. Stummer W et al. Fluorescence-guided surgery with 5-aminolevulinic acid for resection of malignant glioma: a randomised controlled multicentre phase III trial. 7, 392–401 (2006).
9. Stummer W et al. Intraoperative detection of malignant gliomas by 5-aminolevulinic acid-induced porphyrin fluorescence. Neurosurgery 42, 518–25; discussion 525–6 (1998). [PubMed: 9526986]
10. Stepp H & Stummer W 5-ALA in the management of malignant glioma. Lasers Surg. Med 50, 399–419 (2018). [PubMed: 29737540]
11. Coburger J et al. Tumor detection with 5-aminolevulinic acid fluorescence and Gd-DTPA–enhanced intraoperative MRI at the border of contrast-enhancing lesions: a prospective study based on histopathological assessment. Neurosurg. Focus (2014). doi:10.3171/2013.11.FOCUS13463
12. Teraphongphom N, Kong CS, Warram JM & Rosenthal EL Specimen mapping in head and neck cancer using fluorescence imaging. Laryngoscope Investig. Otolaryngol 2, 447–452 (2017).
13. Frangioni JV In vivo near-infrared fluorescence imaging. Curr. Opin. Chem. Biol 7, 626–34 (2003). [PubMed: 14580568]
14. Kim Y et al. Endoscopic imaging using surface-enhanced Raman scattering. Eur. J. Nanomedicine 9, (2017).
15. Blomfield J & Farrar JF The fluorescent properties of maturing arterial elastin. Cardiovasc. Res 3, 161–70 (1969). [PubMed: 5346452]
16. Zhang DY, Singhal S & Lee JYK Optical Principles of Fluorescence-Guided Brain Tumor Surgery: A Practical Primer for the Neurosurgeon. Neurosurgery (2018). doi:10.1093/neuros/nyy315
17. Dijkstra BM et al. SSTR-2 as a potential tumour-specific marker for fluorescence-guided meningioma surgery. Acta Neurochir. (Wien) 160, 1539–1546 (2018). [PubMed: 29858948]
18. Rosenthal EL et al. Safety and Tumor Specificity of Cetuximab-IRDye800 for Surgical Navigation in Head and Neck Cancer. Clin. Cancer Res 21, 3658–3666 (2015). [PubMed: 25904751]
19. Elliott JT et al. Simultaneous in vivo fluorescent markers for perfusion, protoporphyrin metabolism and EGFR expression for optically guided identification of orthotopic glioma HHS Public Access. Clin Cancer Res 23, 2203–2212 (2017). [PubMed: 27799250]
20. Miller SE et al. First-in-human intraoperative near-infrared fluorescence imaging of glioblastoma using cetuximab-IRDye800. J. Neurooncol 139, 135–143 (2018). [PubMed: 29623552]
21. Predina JD et al. Intraoperative Molecular Imaging Combined With Positron Emission Tomography Improves Surgical Management of Peripheral Malignant Pulmonary Nodules. Ann. Surg 266, 479–488 (2017). [PubMed: 28746152]

22. Predina JD, Newton A, Deshpande C, Low P & Singhal S Utilization of targeted near-infrared molecular imaging to improve pulmonary metastasectomy of osteosarcomas. J. Biomed. Opt 23, 1 (2018).
23. Onda N, Kimura M, Yoshida T & Shibutani M Preferential tumor cellular uptake and retention of indocyanine green for in vivo tumor imaging. Int. J. Cancer 139, 673–682 (2016). [PubMed: 27006261]
24. Lee JYK et al. Intraoperative Near-Infrared Optical Imaging Can Localize Gadolinium-Enhancing Gliomas during Surgery. Neurosurgery (2016). doi:10.1227/NEU.0000000000001450
25. Cho SS, Salinas R & Lee JYK Indocyanine-Green for Fluorescence-Guided Surgery of Brain Tumors: Evidence, Techniques, and Practical Experience. Front. Surg 6, 11 (2019). [PubMed: 30915339]
26. Lee JYK et al. Near-infrared fluorescent image-guided surgery for intracranial meningioma. J. Neurosurg 128, 380–390 (2018). [PubMed: 28387632]
27. Lee JYK et al. Intraoperative Near-Infrared Optical Contrast Can Localize Brain Metastases. World Neurosurg. 106, 120–130 (2017). [PubMed: 28669877]
28. Cho SS et al. Intraoperative near-infrared imaging with receptor-specific versus passive delivery of fluorescent agents in pituitary adenomas. J. Neurosurg 1–11 (2018). doi:10.3171/2018.7.JNS181642
29. Jeon JW et al. Near-Infrared Optical Contrast of Skull Base Tumors During Endoscopic Endonasal Surgery. Oper. Neurosurg 17, 32–42 (2019).
30. Baumann BC, Dorsey JF, Benci JL, Joh DY & Kao GD Stereotactic intracranial implantation and in vivo bioluminescent imaging of tumor xenografts in a mouse model system of glioblastoma multiforme. J. Vis. Exp (2012). doi:10.3791/4089
31. Dsouza AV, Lin H, Henderson ER, Samkoe KS & Pogue BW Review of fluorescence guided surgery systems: identification of key performance capabilities beyond indocyanine green imaging. J. Biomed. Opt 1, (2016).
32. Cho SS et al. Comparison of Near-Infrared Imaging Camera Systems for Intracranial Tumor Detection. Mol Imaging Biol 20, 213–220 (2018). [PubMed: 28741043]
33. Roberts DW et al. Coregistered fluorescence-enhanced tumor resection of malignant glioma: relationships between δ-aminolevulinic acid–induced protoporphyrin IX fluorescence, magnetic resonance imaging enhancement, and neuropathological parameters. J. Neurosurg 114, 595–603 (2011). [PubMed: 20380535]
34. Mayhan WG Cellular mechanisms by which tumor necrosis factor-alpha produces disruption of the blood-brain barrier. Brain Res. 927, 144–52 (2002). [PubMed: 11821008]
35. Kobayashi M, Shimizu Y, Shibata N & Uchiyama S Gadolinium enhancement patterns of tumefactive demyelinating lesions: correlations with brain biopsy findings and pathophysiology. J. Neurol 261, 1902–1910 (2014). [PubMed: 25034274]
36. Reyes R et al. Role of tumor necrosis factor–α and matrix metalloproteinase–9 in blood-brain barrier disruption after peripheral thermal injury in rats. J. Neurosurg 110, 1218–1226 (2009). [PubMed: 19199470]
37. Hitti FL & Lee JYK Endoscopic Resection of an Intraventricular Tumor With Second Window Indocyanine Green: 2-Dimensional Operative Video. Oper. Neurosurg. (Hagerstown, Md.) 15, E53–E54 (2018).
38. Cho SS et al. Comparison of Near-Infrared Imaging Camera Systems for Intracranial Tumor Detection. Mol. Imaging Biol 20, 213–220 (2018). [PubMed: 28741043]
39. Roberts DW et al. Red-light excitation of protoporphyrin IX fluorescence for subsurface tumor detection. J. Neurosurg 128, 1690–1697 (2018). [PubMed: 28777025]
40. Kaibori M et al. Intraoperative detection of superficial liver tumors by fluorescence imaging using indocyanine green and 5-aminolevulinic acid. Anticancer Res. 36, 1841–1849 (2016). [PubMed: 27069168]
41. van Dam GM et al. Intraoperative tumor-specific fluorescence imaging in ovarian cancer by folate receptor-alpha targeting: first in-human results. Nat Med 17, 1315–1319 (2011). [PubMed: 21926976]

42. Predina JD et al. A Phase I Clinical Trial of Targeted Intraoperative Molecular Imaging for Pulmonary Adenocarcinomas. Ann. Thorac. Surg 105, 901–908 (2018). [PubMed: 29397932]
43. Predina JD et al. An open label trial of folate receptor-targeted intraoperative molecular imaging to localize pulmonary squamous cell carcinomas. Oncotarget 9, 13517–13529 (2018). [PubMed: 29568374]
44. Predina JD et al. Localization of Pulmonary Ground-Glass Opacities with Folate Receptor–Targeted Intraoperative Molecular Imaging. J. Thorac. Oncol 13, 1028–1036 (2018). [PubMed: 29626619]
45. Predina JD et al. Identification of a Folate Receptor-Targeted Near-Infrared Molecular Contrast Agent to Localize Pulmonary Adenocarcinomas. Mol. Ther 26, 390–403 (2018). [PubMed: 29241970]
46. Roy J, Kaake M & Low PS Small molecule targeted NIR dye conjugate for imaging LHRH receptor positive cancers. Oncotarget 10, 152–160 (2019). [PubMed: 30719210]
47. Lee JYK et al. Review of clinical trials in intraoperative molecular imaging during cancer surgery. J. Biomed. Opt 24, 1–8 (2019).
48. Pagoto A et al. Novel Gastrin-Releasing Peptide Receptor Targeted Near-Infrared Fluorescence Dye for Image-Guided Surgery of Prostate Cancer. Mol. imaging Biol 22, 85–93 (2020). [PubMed: 31025163]
49. Yazaki PJ et al. Improved antibody-guided surgery with a near-infrared dye on a pegylated linker for CEA-positive tumors. J. Biomed. Opt 24, 1 (2019).
50. Maire CL & Ligon KL Molecular pathologic diagnosis of epidermal growth factor receptor. Neuro. Oncol 16 Suppl 8, viii1–6 (2014). [PubMed: 25342599]
51. Keating J et al. Near-Infrared Intraoperative Molecular Imaging Can Locate Metastases to the Lung. Ann. Thorac. Surg 103, 390–398 (2017). [PubMed: 27793401]
52. Valdés PA et al. Quantitative fluorescence using 5-aminolevulinic acid-induced protoporphyrin IX biomarker as a surgical adjunct in low-grade glioma surgery. J. Neurosurg 123, 771–780 (2015). [PubMed: 26140489]
53. Stummer W et al. 5-Aminolevulinic Acid-derived Tumor Fluorescence. Neurosurgery 74, 310–320 (2014). [PubMed: 24335821]

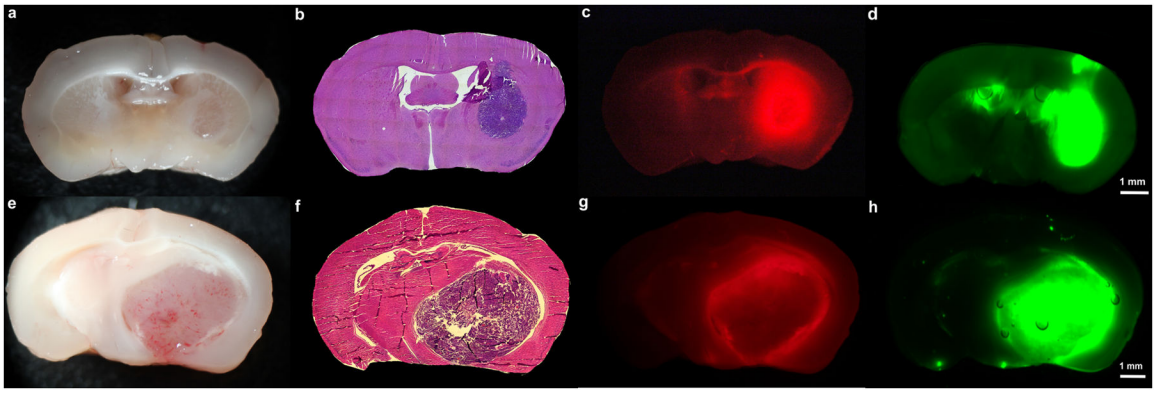

Figure 1: Orthotopic Mouse Glioma Model and Ex-Vivo Fluorescence Imaging.

A-D) PpIX and ICG accumulation in non-necrotic tumors: White-light imaging (A) and H&E staining (B) demonstrates a small, non-necrotic tumor (27.3% of coronal section) in the right hemisphere of this mouse with an orthotopic, U87 tumor. 5-ALA and SWIG were administered to this mouse. Under 400nm excitation and 610–690nm emission for protoporphyrin-IX (C), strong PpIX fluorescence is seen throughout the tumor and corpus callosum, resulting in PpIX fluorescence in 29.3% of the cross-sectional area. Under 785nm excitation (D), strong ICG fluorescence is detected throughout the tumor. There is also non-specific fluorescence seen in the ipsilateral and contralateral ventricles, as well as in the right cortex, resulting in ICG fluorescence in 32.7% of the cross-sectional area. On H&E staining, the ventricles and corpus callosum are devoid of neoplastic cells. In the right cortex, few cells with dark nuclei were seen, but their morphology suggested the presence of inflammatory cells rather than neoplastic cells. This was likely in response to the needle tract made for the intracranial implantation.

E-H) PpIX and ICG accumulation in necrotic tumors: White-light imaging (E) and H&E staining (F) demonstrates a large, necrotic tumor (44.2% of coronal section) in the right hemisphere of this mouse with an orthotopic, GL261 tumor. 5-ALA and SWIG were administered to this mouse. PpIX fluorescence (G) is seen in the peripheral areas of the tumor but not in the tumor core, where there is a significant amount of hemorrhage and necrosis, resulting in positive fluorescence in only 35.5% of the cross-sectional area. In contrast, ICG fluorescence (H) is observed throughout the tumor, even in the necrotic core, resulting in positive fluorescence in 45.2% of the cross-sectional area.

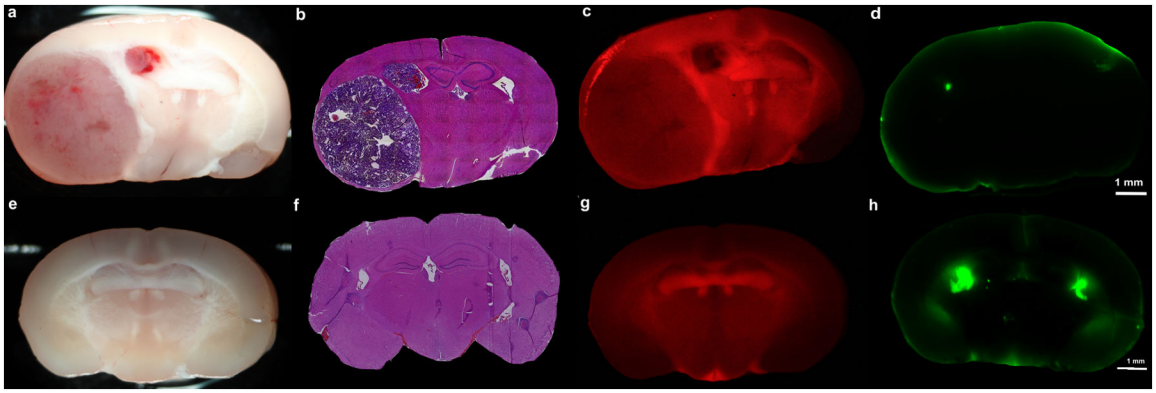

Figure 2: Non-Tumor Areas of Fluorescence under Near-Infrared and Blue-Light Excitation

A-D) Brain autofluorescence: White-light imaging (A) and H&E staining (B) demonstrates a large, necrotic tumor (43.7% of coronal section) in the right hemisphere of this mouse with an orthotopic, GL261 tumor. This mouse did not receive any 5-ALA or SWIG, in order to investigate the presence of autofluorescence under blue-light excitation and NIR excitation. Under 400nm excitation and 610–690nm emission (C), diffuse autofluorescence is seen throughout the brain. The overall signal intensity, however, is 8-fold lower than in the mice that received 5-ALA (8-stops on Canon imaging system). Under 785nm excitation (D), no areas of autofluorescence is seen.

E-H) PpIX and ICG accumulation in control brain: White-light imaging (E) and H&E staining (F) demonstrates a normal brain with no neoplasm in this control mouse. 5-ALA and SWIG were administered to this mouse. Strong PpIX fluorescence is seen in the hippocampal formation, while the corpus callosum demonstrates moderate PpIX fluorescence (G); the overall fluorescence intensity is 4-fold lower than in tumor-bearing mice that received 5-ALA. Strong ICG fluorescence is observed in the lateral ventricles bilaterally and moderate fluorescence is seen in the third ventricle and the horns of the lateral ventricles (H); H&E staining reveals the choroid plexus in these locations.

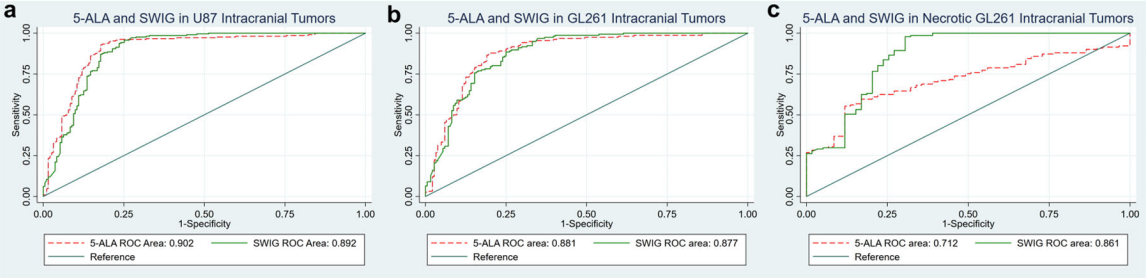

Figure 3: Fluorescence Imaging Accuracy for Detecting Neoplastic Tissue with 5-ALA and SWIG in Murine HGG Model with U87 and GL261 Cell Lines

A) In the 20 coronal slices obtained from U87 tumor-bearing mice, 5-ALA and SWIG had similar accuracies (90.2% vs 89.2%, p-value=0.52)

B) In the 17 coronal slices from non-necrotic GL261 tumor-bearing mice, 5-ALA and SWIG had similar accuracies (88.1% vs 87.7%, p-value=0.83)

C) In the 10 coronal slices from necrotic GL261 tumor-bearing mice, 5-ALA had significantly lower accuracy compared to SWIG (71.2% vs 86.1%, p-value<0.0001).

Overall, the only significant difference between 5-ALA and SWIG in tumor distribution was seen in areas of necrosis mixed in with neoplastic tissue.

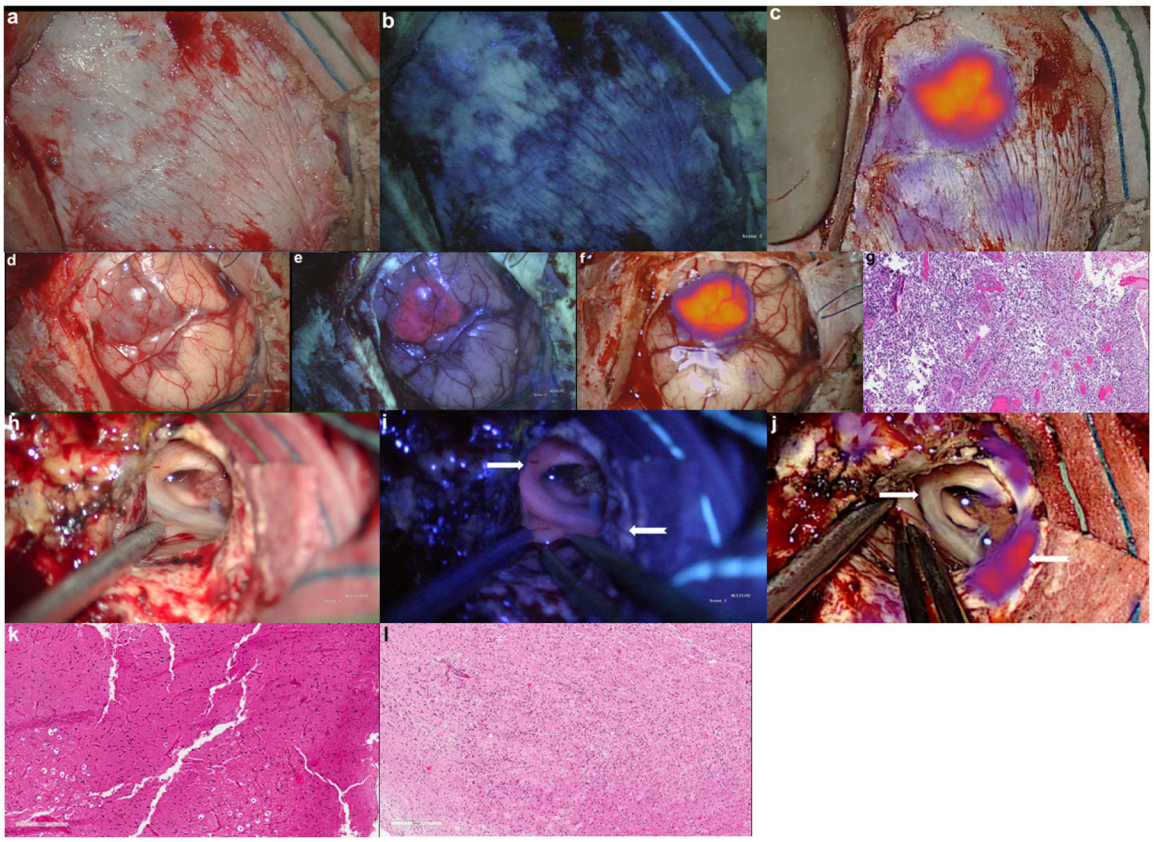

Figure 4: 5-ALA and SWIG Dual-Fluorophore Administration and Intraoperative Visualization.

A 76-year-old female patient undergoing primary resection of a high-grade glioma was administered both 5-ALA and SWIG.

A-C) Intraoperatively, white-light and fluorescence imaging was performed over the intact dura. White-light imaging (A) did not demonstrate any areas suspicious for underlying neoplasm. Blue-light excitation (B) did not elicit any red-fluorescence suggestive of neoplasm. NIR excitation (C), however, localized an area of ICG accumulation consistent with the area of neoplasm.

D-G) Upon durotomy, the tumor was visualized under white-light (D) as a hypervascular and red mass extending to the cortex. Blue-light excitation (E) elicited strong PpIX fluorescence in the area consistent with neoplasm on white-light imaging. Similarly, NIR excitation (F) detected an area of ICG accumulation in the same location that was visualized over the intact dura in (C). A biopsy specimen from this gross tumor demonstrated high-grade glioma cells on histopathology (G).

H-L) In another patient with recurrent HGG, two specimens demonstrated discrepancies between SWIG and 5-ALA fluorescence. One white-matter specimen (white arrow) demonstrated strong red fluorescence (I) but no NIR fluorescence (J). This specimen did not contain any neoplastic cells on histopathology (K). Another specimen (white, notched arrow) demonstrated no PpIX fluorescence (I) but strong NIR fluorescence (J). On histopathology, this specimen contained neoplastic cells mixed in with necrotic tissue (L).

Table 1 -

Biopsy specimens in patients with HGG who received both 5-ALA and SWIG

Subject ID	Age/Gender	Primary or Recurrent	Anatomic Location	White-Light Tumor (Yes/No)	5-ALA (0–2)	SWIG (SBR)	Pathology
323	53/M	Recurrent	Frontal	Yes	2	7.8	GBM – IDH WT
323	53/M	Recurrent	Frontal	Yes	2	10.0	GBM – IDH WT
323	53/M	Recurrent	Frontal	No	2	8.8	GBM – IDH WT
323	53/M	Recurrent	Frontal	***No***	***0***	***2.4***	***GBM – IDH WT***
323	53/M	Recurrent	Frontal	***No***	***2***	***1.3***	***Reactive brain parenchyma***
323	53/M	Recurrent	Frontal	Yes	2	4.0	GBM – IDH WT
331	76/F	Primary	Frontal	No	0	1	Necrosis
331	76/F	Primary	Frontal	Yes	2	6.2	GBM – IDH WT
331	76/F	Primary	Frontal	Yes	2	16	GBM – IDH WT
331	76/F	Primary	Frontal	No	2	6.6	GBM – IDH WT
331	76/F	Primary	Frontal	No	2	3.0	GBM – IDH WT
350	60/M	Primary	Temporal	No	2	2.2	Incidental Meningioma
350	60/M	Primary	Temporal	No	0	1.3	Brain parenchyma
350	60/M	Primary	Temporal	Yes	2	5.5	GBM – IDH WT
350	60/M	Primary	Temporal	Yes	2	11	GBM – IDH WT
350	60/M	Primary	Temporal	No	2	6.6	GBM – IDH WT
350	60/M	Primary	Temporal	No	1	5.5	GBM – IDH WT
360	65/F	Primary	Temporal	Yes	2	6.3	GBM – IDH WT
360	65/F	Primary	Temporal	No	1	3.5	GBM – IDH WT
360	65/F	Primary	Temporal	No	0	1	Reactive brain parenchyma

Table 2 -

Clinical Characteristics of 5-ALA and SWIG

Characteristic	**5-ALA**	**Second Window ICG**
Excitation/Emission Spectrum	400–410nm / 635nm	805nm / 835nm
Route of Administration	Oral	Intravenous
Timing of Administration	3–4 hours Preoperative	24 hours Preoperative
Major Contraindications	Porphyria, Pregnancy	Iodide Allergy, Pregnancy
Adverse Events	Photosensitivity for 2–3 Days Postoperatively	Infusion Site Irritation, Urticaria
Preclinical Tumor Accuracy	80.5%	89.0%
Fluorescence within Necrotic Tissue	Minimal	Equivalent to Neoplastic Tissue
Tumor Visualization through Intact Dura or Tissue	Not possible	Possible
Real-time Overlay of Fluorescence Signal	Not commercially available	Available
Visibility through Optics of Neurosurgical Microscopes	Yes	No